STUDY OF MECHANICAL PROPERTIES OF NANOLAYERED Ti/Ni COATINGS

ZÁBRANSKÝ Lukáš[1], VÁCLAVÍK Richard[1], PŘIBYL Roman[1], ŽENÍŠEK Jaroslav[1],
SOUČEK Pavel[1], BURŠÍK Jiří[2], FOŘT Tomáš[3], BURŠÍKOVÁ Vilma[1]

[1]Department of Physical Electronics, Faculty of Science, Masaryk University, Brno, Czech Republic, EU
[2]Institute of Physics of Materials, Academy of Sciences of the Czech Republic, Brno, Czech Republic, EU
[3]Institute of Scientific Instruments, Czech Academy of Sciences, Brno, Czech Republic, EU

Abstract

The aim of the present work was to study the dependence of mechanical properties of Ti/Ni multilayer thin films on the thicknesses of constituent Ti and Ni layers. The multilayer thin films were synthesized by deposition of Ti and Ni layers alternately on single crystalline silicon substrates using direct current magnetron sputtering method. Thicknesses of Ti and Ni layers varied from 1.7 nm to 100 nm. The micro-structure of the multilayer films was studied using X-ray diffraction technique, scanning electron microscopy with focused ion beam technique and transmission electron microscopy. Mechanical properties obtained from nanoindentation experiments were discussed in relation to microstructural observations.

Keywords: Ti/Ni, multilayers, magnetron sputtering, nanoindentation, TEM

1. INTRODUCTION

TiNi shape memory alloy (so-called nitinol) exhibits two closely related properties: shape memory effect (SME) and superelasticity (SE), which are derived from a martensitic transformation from a simple cubic structure (austenitic, B2 phase) to a monoclinic crystal structure (martensite, B19' phase). This phase transformation is reversible and instantaneous. Due to twinning [1,2], the B19' phase can withstand a limited deformation, which is recovered after transformation to B2 phase and the original shape of the sample is restored and self-healed. The transformation can be achieved by annealing [3,4] or by applying stress [5-7]. Thanks to the SE and SME properties, TiNi alloys has considerable technological relevance - they can be used in medical applications such as artificial bone joints [8,9] or as sensors and actuators in MEMS [10,11].

The nanoindentation technique is a promising method how to study the SE, SME or the phase transformation processes at nanoscale. In the past years, researchers employed both Berkovich [12-14] and spherical [15,16] indenters to study the mechanical properties of TiNi material in both bulk and thin film forms. It was shown that residual idents made with spherical indenter can be fully recovered upon annealing to 400 °C [16] because by using blunter tips the TiNi material is deformed primarily via strain-induced phase transformation and the plastic deformation plays minor role.

For MEMS application it is necessary to produce TiNi thin films with thickness of several μm, for which standard methods of production as rolling and melt-spinning are unsuitable and insufficient. The TiNi thin films with low thickness are thus mainly synthesized by DC magnetron sputtering of a TiNi target [17]. On the other hand, other methods as e-beam evaporation [18] or pulsed laser deposition [19] are reported. Although TiNi thin films deposited by DC magnetron sputtering exhibit excellent SME and good mechanical properties, the martensitic transformation temperature of TiNi SME is strongly affected by chemical composition [20] which cannot be perfectly controlled by using these conventional methods. As an alternative, which controls the chemical composition more precisely, the dual-head sputtering system with Ti and Ni targets can be utilized for fabrication of Ti/Ni multilayer films consisting of alternating nanolayers of pure Ti and Ni. Afterwards, this system can be converted into the TiNi alloy thin film through solid state amorphization by using a heat treatment [21-24]. The final chemical composition is controlled by the deposition time of an individual nanolayer which

sets its individual thickness. By using this fabrication method, the resulting TiNi shape memory alloy has comparable mechanical properties and its SME occurs for lower temperatures compared to TiNi prepared by sputtering of a single TiNi target [25].

In this study we focused on the evaluation of mechanical properties of Ti/Ni multilayers prepared by dual-head magnetron sputtering of Ti and Ni targets. Coatings composed of nanolayers of Ti and Ni with different individual thicknesses were compared by means of nanoindentation with Berkovich tip. The grain size was calculated from X-ray diffraction. The deformed area of the residual indents was analyzed in cross-sections by combination of focused ion beam (FIB) and post-mortem transmission electron microscopy (TEM) techniques and the prevailing deformation mechanism was found.

2. EXPERIMENTAL

A set of Ti/Ni multilayered coatings with different thicknesses of individual Ti or Ni layers were prepared by magnetron sputtering of titanium and nickel targets in an argon atmosphere. Prior to the deposition the single crystalline silicon substrates were cleaned and etched by ion bombardment for 5 minutes. The floating potential on a substrate holder was used and the substrate rotation was turned on to ensure good spatial homogeneity and constant thickness of individual layers. The deposition conditions as applied power on targets, deposition pressure and substrate rotation speed are presented in **Table 1** for each design of Ti/Ni multilayered coatings. During the deposition the power on targets were periodically turned on and off depending on which layer was currently deposited. The growth rates of Ti and Ni were found to be 0.75 nm/s and 1.52 nm/s, respectively, and the deposition time varied depending on the desired thickness of an individual layer h. The first described film in the **Table 1** is composed of Ti + Ni without multilayered microstructure and was synthesized by sputtering of Ti and Ni targets together.

Table 1 Summary of deposition conditions for all designs of Ti/Ni multilayered coatings.

h [nm]	Overall thickness [nm]	Power on Ti target [W]	Power on Ni target [W]	Deposition pressure [Pa]	Rotation [rpm]
No multilayer	500	350	350	0.30	3.0
100	500	350	350	0.30	3.0
50	500	350	350	0.30	3.0
10	500	350	350	0.30	3.0
5.0	1000	300	200	0.16	4.8
2.5	1000	300	300	0.16	4.8
1.7	1200	300	300	0.16	4.8

The depth sensing nanoindentation method performed on Hysitron TI950 Triboindenter equipped with a Berkovich tip was used for measurement of indentation hardness and reduced elastic modulus. The mounted nanoscale measuring head with resolution of 1 nN and load noise floor lower than 30 nN allow to measure in the load range from 50 nN up to 11 mN. Several quasistatic tests, each containing 20 segments of partial unloading which provided hardness and modulus as functions of indentation depth, were carried out in load controlled regime using a constant loading rate of 0.2 mN/s. The partial unloading segments were fitted and evaluated according to standard procedure proposed by Oliver and Pharr [26] and values of indentation hardness and reduced elastic modulus were obtained from a region where the substrate influence as well as tip rounding and surface effects were negligible.

The micro-indentation tests used for microscopic evaluation of deformed area were performed by a Berkovich tip (tip radius ~ 200 nm) with applied load of 1 N. Thin lamellar cross sections for TEM observations on a Philips CM12 STEM transmission electron microscope operating at 120 kV and a JEOL 2100F high resolution TEM

were prepared using a focused ion beam in Tescan LYRA 3 XMU SEM x FIB scanning electron microscope. The measurements of X-ray diffraction (XRD) were performed on a Rigaku Smartlab X-ray diffractometer with a grazing angle of incidence configuration and the grain sizes for Ti and Ni layers were calculated using Scherrer formula [27].

3.   RESULTS AND DISCUSSION

The XRD patterns presented in **Figure 1** show polycrystalline microstructure of Ti/Ni multilayers. The microstructure is composed of hexagonal (hcp) Ti and cubic (fcc) Ni grains of different sizes. For the case of Ti/Ni system with thick layers (here 50 nm), dominant reflections from a hcp Ti lattice (002) and from fcc Ni lattice (111) and (200) were observed. For thinner layers, the Ti (002) peak gets wider and for h = 2.5 nm it disappears. For h = 5 nm, another peak emerged at 41.4 ° for which the reflection of Ti (101) is responsible. This peak also contributes to the observed wide band observed for the sample with h = 2.5 nm. With decreasing the individual layer thickness h, a peak broadening is obvious for Ti as well as for Ni layers indicating finer grains for thinner layers. For smaller thickness of an individual layer, the grain growth is suppressed and finer grains are dominant.
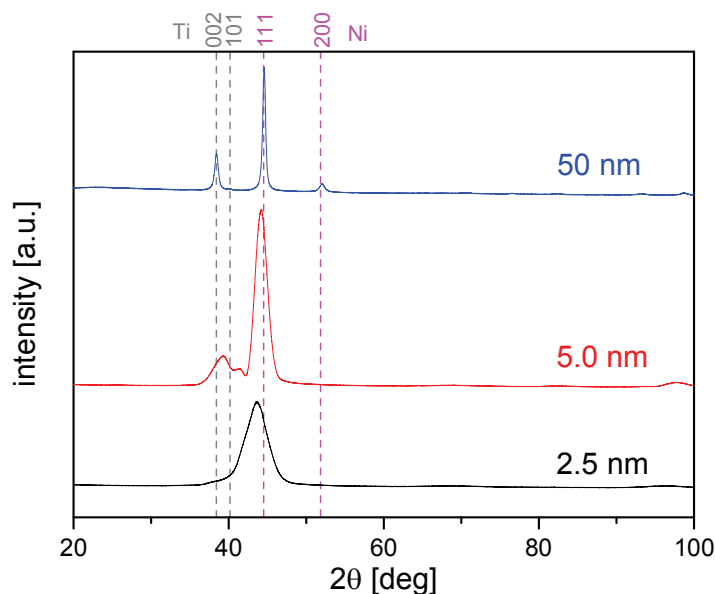
Figure 1 Diffraction patterns for Ti/Ni multilayers with individual layer thickness h = 50, 5.0 and 2.5 nm

The dependencies of grain sizes of individual Ti and Ni layers are presented in **Figure 2**. The mean grain size gradually decreases with decreasing h from ~ 15 nm for h = 100 nm down to ~ 3 nm for h = 2.5 nm of thickness. The diffraction peaks Ti (002) and Ni (111) for samples with layers of 2.5 and 1.7 nm thickness were overly wide so the precise calculation of mean grain size was difficult and presented values are only estimations.

The evolution of hardness as a function of h is plotted in **Figure 3**. The layer with thickness of 0 nm was assigned to the Ti + Ni sample without the multilayered microstructure. Hardness increases with decreasing the layer thickness from 100 nm down to 10 nm. While the peak hardness of ~ 9 GPa was reached at 10 nm, which is in accordance with literature [28], a gradual drop of hardness is observed for further decrease of h. Generally, for polycrystalline multilayer thin films, both fine grains and small individual layer thickness can contribute to material strengthening due to dislocation-mediated deformation mechanisms. The evolution of hardness in the thickness region between 100 nm and 10 nm can be described and explained by Hall-Petch mechanism [29, 30], which states that material with finer grains contains more grain boundaries providing more barriers to dislocation movement.
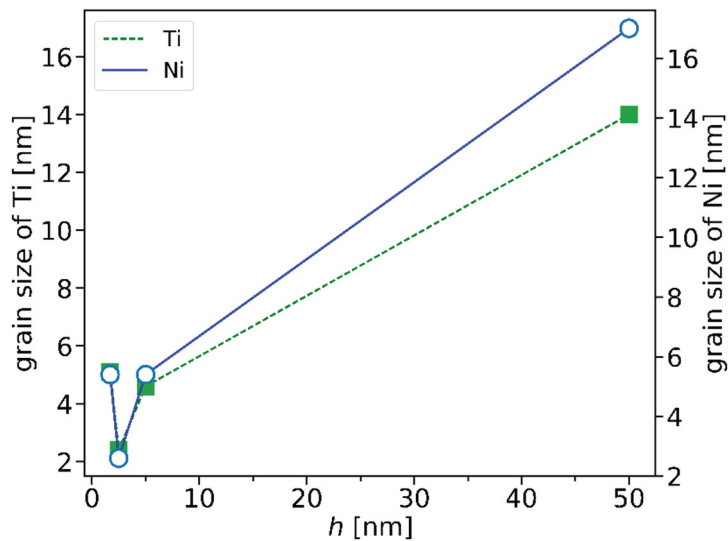
Figure 2 The mean grain size evolutions for Ti and Ni grains calculated by Scherrer formula
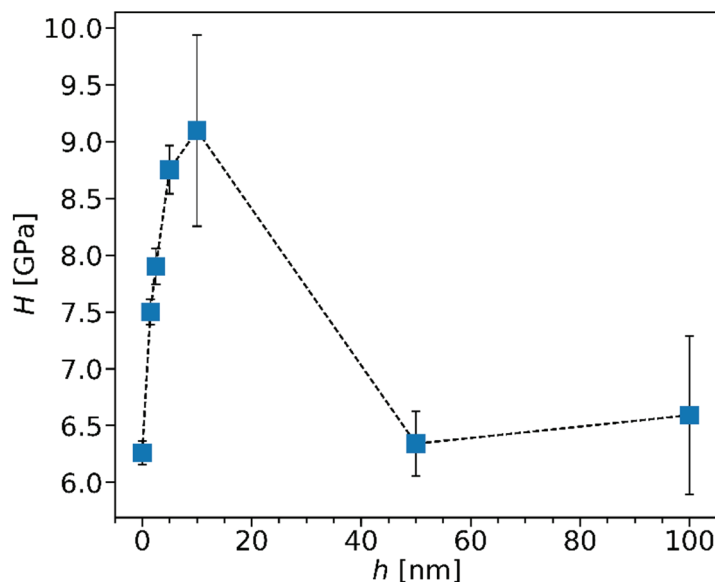
Figure 3 The dependency of hardness H on individual layer thickness h

The Hall-Petch mechanism can also be applied for multilayered systems if the grain size in the Hall-Petch equation is replaced by the individual layer thickness [28, 31]. The dislocation strengthening is then caused by dislocation pile-up on interfaces between individual layers. System with thinner layers then correspondingly suppress more easily the dislocation motion than multilayers consisting of thicker layers. The empirical Hall-Petch mechanism is applicable for layers of thickness higher than 50 nm. In the range of approximately 10 - 100 nm [28, 32, 33], the dominant deformation mechanism is confined layer slip which is based on a single dislocation bowing between two interfaces. Both, Hall-Petch law and confined layer slip mechanisms, predicts the hardness increase with decreasing h.

The hardness in the region $h > 10$ nm gradually decreases. This behavior can be interpreted as a shift from confined layer slip deformation mechanism to interface crossing of single dislocations [28]. In **Figure 4** a cross-sectional TEM image from the deformed region after a 1 N micro-indentation is presented for a multilayered coating with $h = 5$ nm from which it is clear that interfaces near the deformed region are smeared and broken which supports the explanation of dislocation motion through interfaces. The resistance of an interface to

transmission of a single glide dislocation is largely independent of h and decreases only if the layer thickness approaches the size of dislocation core dimension (approximately ~ 1 nm) [33, 34]. However, in this situation the onset of the hardness decrease is at h between 5 and 10 nm which is higher than the typical size of a dislocation core. Therefore, although the glide dislocation motion through interfaces may be a partial explanation of hardness drop for very low layer thicknesses, other mechanisms need to be sought for.
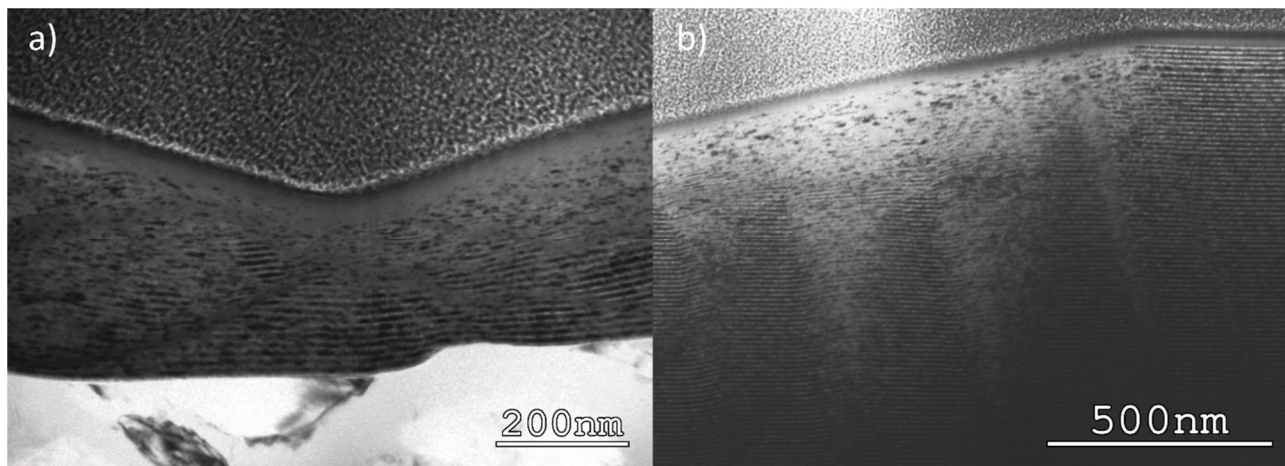
Figure 4 The cross-sectional transmission electron microscopy images of a) central region and b) edge of the deformed area under the micro-indentation imprint for the sample with layer thickness h = 5.0 nm

As it was shown by XRD (see **Figures. 1 and 2**), the Ti/Ni multilayers exhibited a polycrystalline microstructure with the mean grain size increasing with h and, thus, a grain boundary sliding can be considered as another softening mechanism. Also, a slight stress induced recrystallization of Ti and Ni to nitinol (TiNi) close to the interface can introduce a new stress which can lead to subsequent decrease of interfacial resistance to dislocation transmission (see **Figure 4**) resulting in the observed decrease of hardness.

4. CONCLUSION

Several Ti/Ni multilayers with different individual thickness of Ti and Ni layers were synthesized by magnetron sputtering. From the XRD results it was concluded that all synthesized coatings have polycrystalline microstructure and that the mean grain size decreased gradually for thinner layers. The hardness evolution with layer thickness was explained in detail. The maximum value of 9 GPa was found for the individual thickness of 10 nm. For higher thicknesses down to 10 nm, the changes in hardness follow rules of Hall-Petch and confined layer slip mechanisms. The decrease of hardness for thicknesses below 10 nm was explained by a combination of several factors. While for very small thicknesses the transmission of single glide dislocation is dominant, for thicknesses in the region between 5 to 10 nm, where the onset of the hardness decrease lies, other mechanisms as grain boundary sliding within individual layers or stress induced recrystallization to TiNi play more important role.

ACKNOWLEDGEMENTS

REFERENCES

[1]   EZAZ, T., SEHITOGLU, H., *Appl. Phys. Lett.,* 2011, vol. 98, pp. 141906

[2]   EZAZ, T., SEHITOGLU, H., MAIER, H.J., *Acta Mater.,* 2011, vol. 59, pp. 5893

[3]   PAN, G., CAO, Z., SHI, J., WEI, M., XU, L., MENG, X., *Sensors and Actuators A*, 2014, vol. 217, pp. 75-80

[4]   PAN, G., CAO, Z., WEI, M., XU, L., SHI, J., MENG, X., *Mat. Sci. Eng. A*, 2014, vol. 600, pp. 8-11

[5]   PFETZING-MICKLICH, J., SOMSEN, Ch., DLOUHY, A., BEGAU, Ch., HARTMAIER, A., WAGNER, M.F.X., EGGELER, G., *Acta Mater.*, 2013, vol. 61, pp. 602-616

[6]   OTSUKA, K., WAYMAN, C.M., *Shape memory materials*. New York: Cambridge University Press, 1998

[7]   FUNAKUBO, H., *Shape memory alloys*. New York: Gordon & Breach, 1987

[8]   GIL, F.J., PLANELL, J.A., *Proc. Inst. Mech. Eng. H*, 1998, vol. 212, no. 6, pp. 473-488

[9]   KANG, S., YOON, K., KIM, J., NAM, T., TAE-HYUN, G., GJUNTER, V., *Mater. Trans.*, 2002, vol. 43, pp. 1045-1048

[10]   GILL, J.J., HO, K., CARMAN, G.P., *J. MEMS*, 2002, vol. 11, pp. 68-77

[11]   BHATTACHARYA, K., JAMES, R.D., *J. Mech. Phys. Solids*, 1999, vol. 47, pp. 531-576

[12]   MONTECINOS, S., CUNIBERTI, A., SIMISON, S., *Intermetallics*, 2012, vol. 28, pp. 58-64

[13]   SINHA, A., CHATTOPADHYAY, P.P., *Mater. Sci. Eng. A*, 2012, vol. 552, pp. 540-546

[14]   FRICK, C.P., LANG, T.W., SPARK, K., GALL, K., *Acta Mater.*, 2006, vol. 54, pp. 2223-2234

[15]   KOMVOPOULOS, K., MA, X.G., *Appl. Phys. Lett.*, 2005, vol. 87, pp. 263108

[16]   WOOD, A.J.M., SANJABI, S., FU, Y.Q., BARBER, Z.H., CLYNE, T.W., *Surf. Coat. Technol.*, 2008, vol. 202, pp. 3115-3120

[17]   WASA, K., HAYAKAWA, S., *Handbook of Sputter Deposition Technology*, Pork Ridge, NJ: Noyes Publications, 1992

[18]   ADAMS, T.M., KIRKPATRICK, S.R., WANG, Z., SIAHMAKOUN, A., *Mat. Lett.*, 2005, vol. 59, no. 10, pp. 1161-1164

[19]   CIABATTARI, F., FUSO, F., ARIMONDO, E., *App. Phys. A: Mat. Sci. Proc.*, 2004, vol. 79, no. 4-6, pp. 623-626

[20]   ISHIDA, A., TAKEI, A., MIYAZAKI, S., *Thin Solid Films*, 1993, vol. 228, pp. 210-214

[21]   CLEMENS, B., *J. Appl. Phys.*, 1987, vol. 61, pp. 4525-4529

[22]   LEHNERT, T., TIXIER, S., BÖNI, P., GOTTHARDT, R., *Mater. Sci. Eng. A*, 1999, vol. 273-275, pp. 713-716

[23]   CHO, H., KIM, H.Y., MIYAZAKI, S., *Sci. Tech. Adv. Mater.*, 2005, vol. 6, pp. 678-683

[24]   EMADINIA, O., SIMÕES, S., VIANA, F., VIEIRA, M.F., CAVALEIRO, A.J., RAMOS, A.S., VIEIRA, M.T., *Weld World*, 2016, vol. 60, pp. 337-344

[25]   SAKURAI, J., KIM, J.I., HOSODA, H., MIYAZAKI, S., *Trans. MRS-J.*, 2001, vol. 26, pp. 319-322

[26]   OLIVER, W.C., PHARR, G.M., *J. Mat. Res.*, 2004, vol. 19, pp. 3-20

[27]   SCHERRER, P., *Göttinger Nachrichten Gesell.*, 1918, Vol. 2, pp. 98-100

[28]   YANG, Z., WANG, J., *Micro and Nanomechanics*, 2016, vol. 5, pp. 41-49

[29]   HALL, E.O., *Proc. Phys. Soc. Sec.*, 1951, vol. B64, pp. 747-753

[30]   PETCH, N.J., *J. Iron Steel I.*, 1953, vol. 174, pp. 25-28

[31]   ANDERSON, P.M., LI, C., *Nanostruct. Mater.*, 1995, vol. 5, pp. 349-362

[32]   WANG, J., MISRA, A., *Curr. Opin. Solid St. M.*, 2011, vol. 15, pp. 20-28

[33]   PHILLIPS, M.A., CLEMENS, B.M., NIX, W.D., *Acta Mater.*, 2003, vol. 51, pp. 3178-3184

[34]   WANG, J., HOAGLAND, R.G., HIRTH, J.P., MISRA, A., *Acta Mater.*, 2008, vol. 56, pp. 3109-3119